Femtosecond Laser Regulated Ultrafast Growth of Mushroom-Like Architecture for Oil Repellency and Manipulation

Yi Yang,[§] Yachao Zhang,[§] Yanlei Hu,* Guoqiang Li,* Cong Zhang, Yuegan Song, Longfu Li, Caiding Ni, Nianwei Dai, Yong Cai, Jiawen Li, Dong Wu,* and Jiaru Chu

Cite This: *Nano Lett.* 2021, 21, 9301–9309

Read Online

ACCESS | Metrics & More | Article Recommendations | Supporting Information

ABSTRACT: Natural organisms can create various microstructures via a spontaneous growth mode. In contrast, artificial protruding microstructures are constructed by subtractive methods that waste materials and time or by additive methods that require additional materials. Here, we report a facile and straightforward strategy for a laser-induced self-growing mushroom-like microstructure on a flat surface. By simply controlling the localized femtosecond laser heating and ablation on the poly(ethylene terephthalate) tape/heat-shrinkable polystyrene bilayer surface, it is discovered that a mushroom-like architecture can spontaneously and rapidly grow out from the original surface within 0.36 s. The dimension of the re-entrant micropillar array (cap diameter, pillar spacing, and height) can be accurately controlled through the intentional control of laser scanning. Followed by a fluorination and spray coating, the obtained surface can realize the repellency and manipulation of oil droplets. This work provides new opportunities in the fields of microfabrication, microfluidics, microreactor engineering, and wearable antifouling electronics.

KEYWORDS: *femtosecond laser, self-growth, re-entrant structures, oil manipulation, superamphiphobic surfaces*
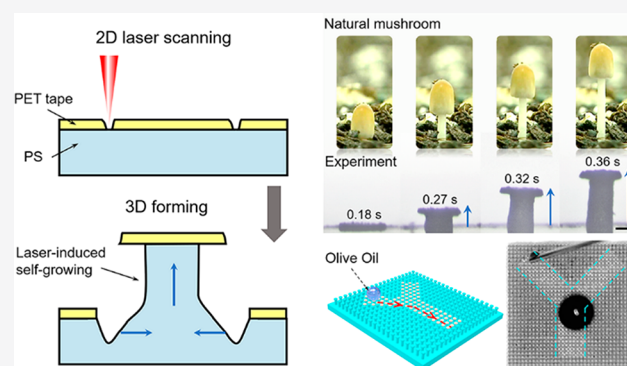
Universally but magically, a seed can grow from the soil to form a standing plant. In contrast to this elegant and autonomous approach in nature, to create a protruding microstructure on a flat substrate, fundamentally different methods have been developed, by subtractive and additive manufacturing methods. For subtractive manufacturing (turning, cutting, milling, grinding, etc.), a large amount of materials around the target microstructures needs to be removed,[1] which inevitably leads to the waste of materials and time. While additive manufacturing (material extrusion, jetting, polymerization, powder bed fusion, etc.) has the advantage of saving time and materials,[2−6] it requires additional material that can be melted or polymerized to deposit on the substrate.[7,8]

Recently, to avoid the above-mentioned drawbacks of conventional methods, green and promising growth strategies have been developed to construct out-of-plane surface topologies based on the mass transport of matrix materials.[9−12] Borer et al.[9,10] combined UV irradiation and heating to form surface relief structures on the blended photopolymer substrates by monomer diffusion and polymerization, where irradiation was applied to generate radicals in the exposed areas, and heating was used to enhance the monomer mobility and polymerization. Xue et al.[11] reported a light-induced strategy for regulating the localized growth of microstructures from the surface of a swollen dynamic substrate, in which

reactions including photolysis, photopolymerization, and transesterification are triggered to drive the monomers trapped in a substrate into the irradiated region to form a protruding structure. Different from the above free radical polymerization methods, Jiang et al.[12] developed a more effective photo-induced growth approach to fabricate ordered functional patterns; that is, light regulates the directional motion and polymerization of maleimide in a diffusion system. These explorations have extensively advanced the development of growth of protruding microstructures on the surface. However, two disadvantages must be considered: (1) These light-regulated monomer local polymerization methods require monomer directional motion and polymerization, which is time-consuming with an extremely low growth speed (average speed less than 50 nm/s). (2) Because of the constraint of matrix materials, only low-aspect ratio surface relief micro-patterns have been successfully fabricated, which hinders applications that require more complex architectures. There-
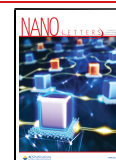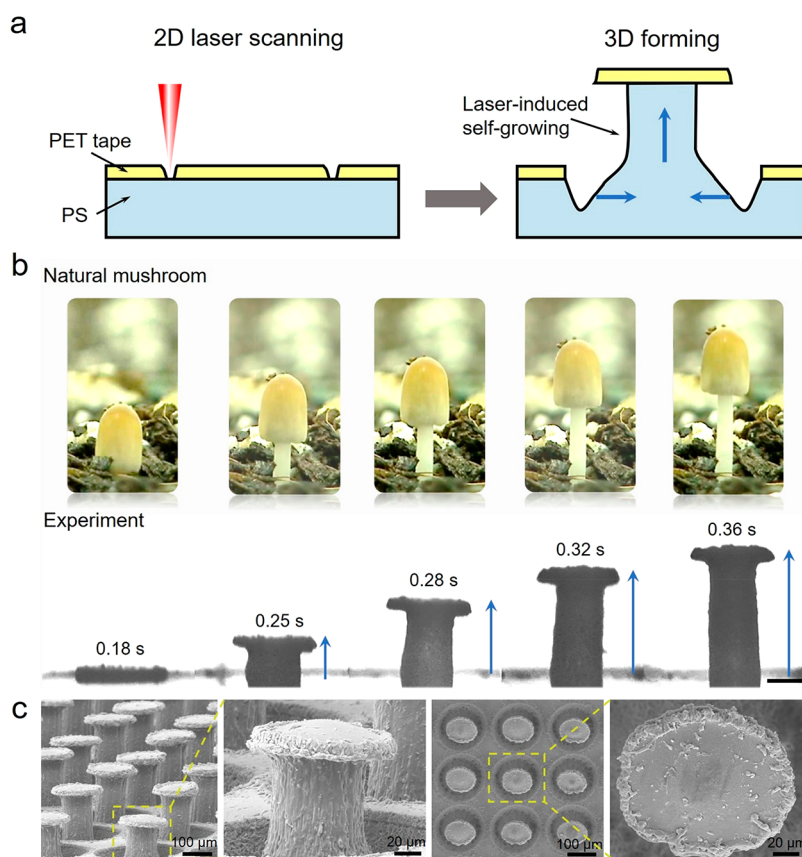
Figure 1. Fabrication and characterization of re-entrant micropillars on a PET tape/PS bilayer. (a) Schematic for laser-induced self-growing re-entrant micropillar. Blue arrows in the sketch indicate the symmetric shrinkage of material in the *x-y* plane and growth in the *z*-direction. (b) Side view of optical images shows the growth of a re-entrant micropillar with an increasing repeat circle, corresponding to the growth of a natural mushroom (*psathyrellaceae*, images courtesy of J. Quinlan). Scale bar: 50 μm. (c) Tilted view and top view of the SEM images of a re-entrant micropillar array.

fore, it is a timely challenge to seek a more direct and efficient way to construct out-of-plane surface structures, which is highly desirable to micro- and nanotechnology.

With the combination of the fascinating deformability of shape-memory polymer (SMP) and femtosecond laser precise processing capability, we proposed a fast laser-induced polymer self-growing method to construct a high-aspect-ratio micropillar on a heat-shrinkable SMP film[13] (only 4 s is needed for a 540 μm high micropillar). Superior to micropillars, a mushroom-like reentrant architecture is considered as a key to realize superamphiphobicity,[5,14−19] which is of paramount significance in microreactor engineering,[20−23] antifouling,[24] oil/water separation,[25,26] and anti-icing.[27] Nevertheless, limited by the rectilinear propagation of light, the microstructures prepared by laser surface processing technology are mainly simple micropillars or microwalls,[28−31] and it has long been considered impossible to directly fabricate a mushroom-like re-entrant structure.

Here, we report a highly efficient method to fabricate re-entrant micropillars via a laser-induced self-growth on the poly(ethylene terephthalate) (PET) tape/polystyrene (PS) bilayer surface. The growth speed is 317 ± 14 μm/s, which is 3 orders of magnitude higher than that of light-regulated monomer polymerization methods. The dimension of the re-entrant micropillar array can be accurately tuned by the intentional control of laser scanning. Followed by a fluorination and spray coating, the hierarchical re-entrant

surface (HRES) exhibits a super-repellency to liquids with a low surface tension such as hexadecane. On this basis, the microchannel is prepared by precisely controlling the height of the re-entrant micropillars, and the manipulation of oil droplets is realized. Last but not least, by taking advantage of the flexibility of a polymeric substrate, the superamphiphobic property can be easily transferred to curved substrates for an efficient oil transportation. Our presented robust, scalable, accurate, and highly efficient approach offers a strategy to design flexible superamphiphobic devices, and it shows promising interdisciplinary potential for microfabrication, microfluidics, microreactor engineering, and wearable electronics.

■ RESULTS AND DISCUSSION

Laser-Induced Self-Growing Mushroom-Like Architecture on a PET tape/PS Bilayer. It has been known that the heat-affected zone where the femtosecond laser interacts with a material can be finely confined and has a sufficiently high temperature, benefiting the localized treatment of the heat-sensitive polystyrene shape memory polymer film.[13,28,32,33] As shown in Figure 1a, a femtosecond laser is employed to continuously scribe preprogrammed 2D circles on a bilayer consisting of an unshrinkable capping PET layer (thickness of 10 μm) and a shrinkable underlying PS layer (thickness of 150 μm). The interaction between laser and bilayer film involves two effects: localized laser ablation and
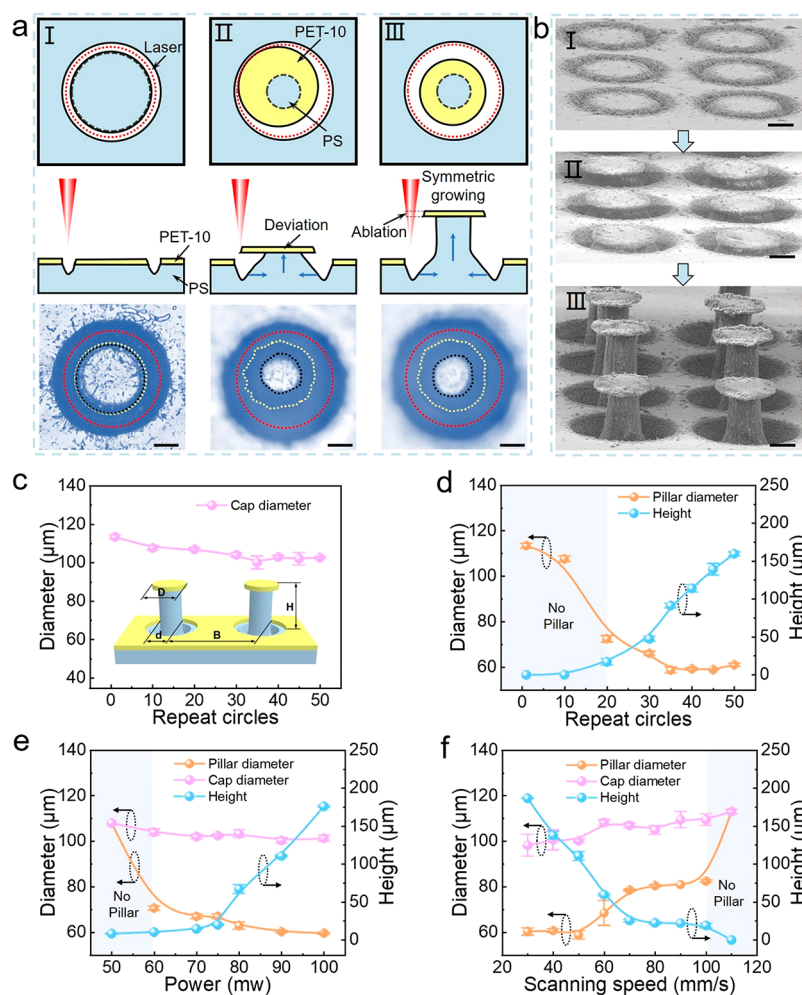
Figure 2. Evolution of re-entrant micropillar and the optimization of processing parameters. (a) Schematic illustration showing three stages during laser-induced re-entrant micropillar self-growth when PET-10 is utilized as a capping layer. The schematics in the upper row and middle row show a top view and cross-sectional profiles of the microstructure, respectively. The red circle indicates the laser scanning path, and blue arrows in the sketch indicate the shrink direction of the material in the *x-y* plane and the increase direction in the *z*-direction. The top view optical images in the lower row show the corresponding microstructures. Scale bars: 30 μm. (b) SEM images show corresponding microstructures of three stages (70° tilted view). Scale bars: 50 μm. (c−f) The quantitative relationship between pillar diameter, pillar height, cap diameter of re-entrant micropillar with repeat circles, power, and scanning speed. Light gray regions indicate no pillar is formed. (inset) Schematic of the re-entrant micropillar, indicating its dimensions.

laser heating, which occur simultaneously during the growth of the re-entrant micropillar. On the one hand, the bilayer of PET/PS inside the circle is separated from the matrix in the *x-y* plane by a laser ablation to release the restraint. On the other hand, as the laser-scanning circles increase, the heat accumulation leads to the shrinkage and growth of the underlying PS when the material reaches the glass transition temperature. But the capping PET layer cannot shrink; thus, the re-entrant micropillar is formed. As shown in Figure 1b and Movie S1, it is fascinating that a three-dimensional (3D) re-entrant micropillar rapidly grows up by a continuous laser scanning within 0.36 s (the average growth velocity is 317 ± 14 μm s^{-1}), corresponding to the intriguing growth of natural mushroom (*psathyrellaceae*). The re-entrant micropillar array is fabricated, and good morphology uniformity is demonstrated in Figures 1c and S1.

The Evolution of Re-Entrant Micropillar and the Optimization of Processing Parameters. Three different capping layers, termed 10 μm thick PET tape (PET-10), 30 μm thick PET tape (PET-30), and 30 μm thick polyimide tape

(PI-30), are chosen to fabricate re-entrant micropillars. It is observed that, only when PET-10 is utilized as a capping layer, the re-entrant micropillars can grow uniformly (Figure S2), while for the PET-30 and PI-30, the re-entrant micropillars tilt randomly (Figures S3 & S4). According to the shape of a microstructure, the growth of a re-entrant micropillar can be divided into three stages, as shown in Figure 2a,b. In stage I, the PET-10 is cut through, and one part of the PS is ablated. However, the heat accumulation is not enough to induce thermal shrinkage. In stage II, the heat accumulation is enough to induce the shrinkage-growth of PS. Because of the low conformal ability between the capping layer and PS (Figure S5), the PET-10 deviates randomly from the original position, and thus the laser beam is partially blocked. Fortunately, the laser can ablate through PET-10 easily within seven scanning circles (Figure S6); therefore, the shrinkage-growth is not influenced, and a re-entrant micropillar grows vertically (stage III). Differently, more scanning circles (22 and 76) are required for PET-30 and PI-30, respectively (Figure S6). Therefore, in stage III for PET-30 and PI-30, the laser is
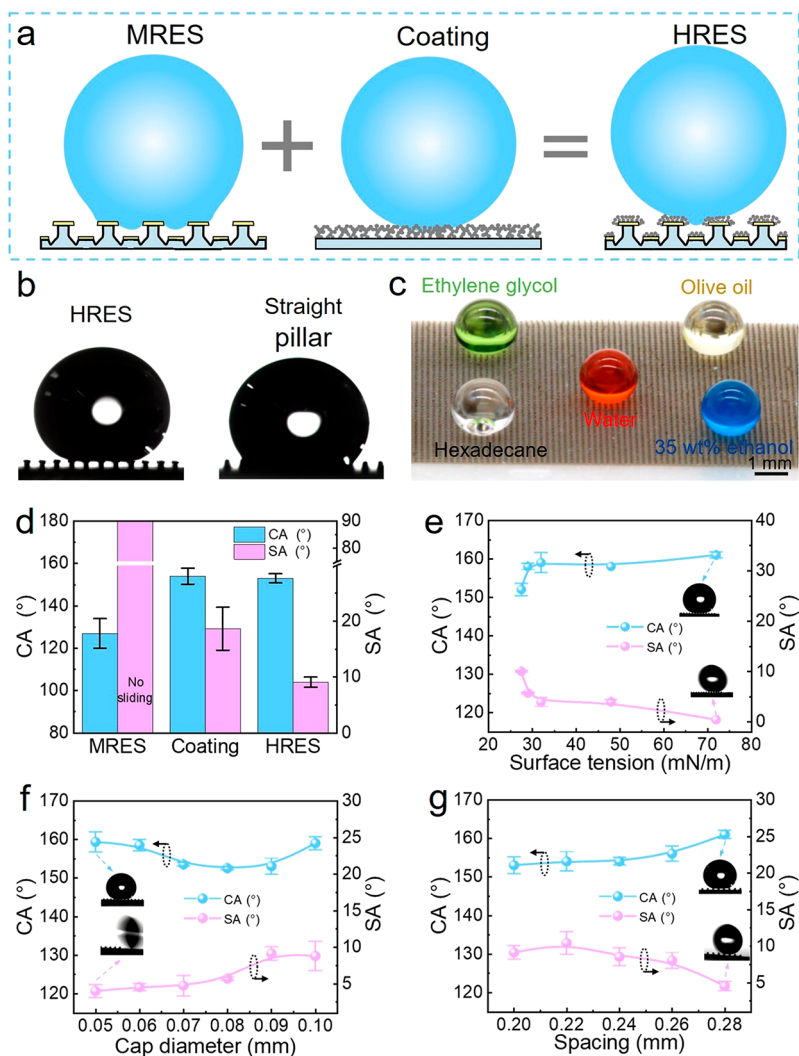
Figure 3. Superamphiphobicity of the HRES. (a) Schematic illustration of the design of HRES. (b) The optical images of a 4 μL olive oil droplet on the HRES and straight pillar surface, respectively. (c) Optical image of five different liquid droplets on the HRES. (d) The contact angle and sliding angle of olive oil (4 μL) on MRES, coating, and HRES, respectively. (e) The contact angle and sliding angle of various liquids as functions of surface tension on the HRES (cap diameter and pillar spacing are 0.1 mm and 0.2 mm, respectively). (f) The contact angle and sliding angle of olive oil (4 μL) on the HRES with different cap diameters (pillar spacing is fixed at 0.2 mm). (g) The contact angle and sliding angle of olive oil (4 μL) on the HRES with different pillar spacing (cap diameter is fixed at 0.09 mm).

partially shaded in the scanning path for a relatively long time, and a tilt re-entrant micropillar is formed because of the asymmetric shrinkage and growth (Figures S7−S10).

Engineering the geometry parameters related to the re-entrant structure (e.g., pillar diameter (d), pillar height (H), cap diameter (D), and pillar spacing (B)) is crucial for an implementation of superamphiphobic surfaces. The inset of Figure 2c shows a schematic of the designed re-entrant structure. The gray regions are utilized to indicate that no re-entrant micropillar is formed in Figure 2d−f. As the repeat circles and laser power increase (Figure 2c−e), the energy provided by the laser increases; thus, the cap diameter decreases and finally stabilizes at ∼100 μm because of the laser ablation. Differently, pillar diameter decreases largely due to the shrinkage and stabilizes at ∼60 μm, coinciding with the macroscale PS film shrinkage ratio limit of 55% (the designed diameter of circular scanning path is 110 μm). Conversely, as the scanning speed increases, the heating time of the laser spot along the scanning path decreases, resulting in a reduction of

the cap ablation and pillar shrinkage (Figure 2f). Accordingly, the pillar height increases with the repeat circle and laser power and decreases with scanning speed (Figure 2c−f).

Superamphiphobicity of the HRES. Inspired by the multilevel structures with a superwettability property in nature,[34,35] an HRES is prepared by spray-coating fluoro-silicon on the fluorinated micro re-entrant surface (MRES) as shown in Figures 3a and S11. To characterize the wettability of the HRES, 4 μL of olive oil and water droplets are deposited on the surfaces, respectively. The contact angle (CA) of olive oil (γ = 32 mN/m) and of water (γ = 72.8 mN/m) on the HRES is 153 ± 2.1° and 163 ± 2°, respectively (Figures 3b and S12). For the surface consisting of straight micropillars with the same pillar diameter and height (the only difference is that the straight micropillars have no caps), the contact angle of water is 159 ± 1° (Figure S12), whereas the olive oil droplet permeates into the straight micropillar array (contact angle is 126 ± 1°), demonstrating the key role of the re-entrant topography (Figure 3b).
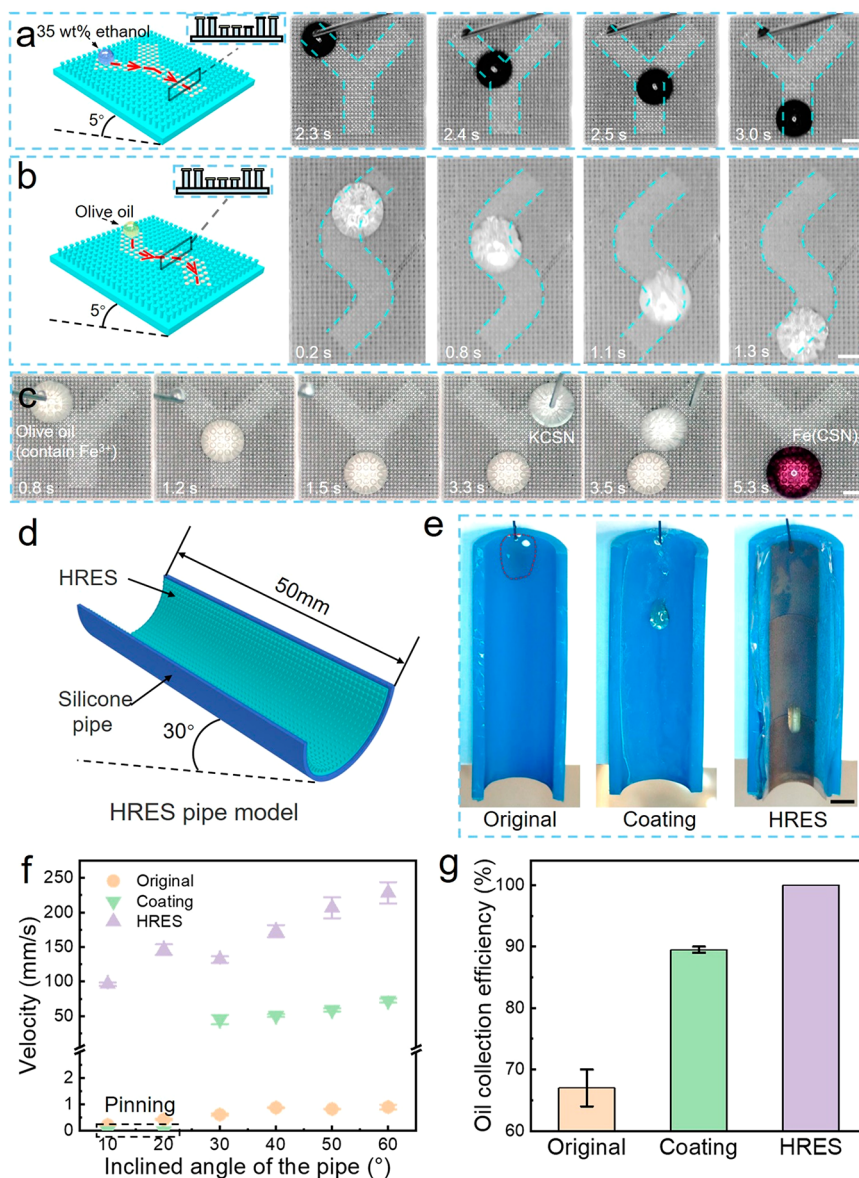
Figure 4. Controllable oil manipulation on the flexible HRES. (a) Droplet of 35 wt % ethanol dyed with a methylene blue solution rolls along the designed Y-type channel (tilt angle is 5°). (b) Droplet of olive oil rolls along the designed S-type channel (tilt angle is 5°). The cross-sectional profiles of the schematics in (a, b) show that the height of the re-entrant micropillar in the channel is lower than that of the surrounding region. (c) Microsampling detection on the designed Y-type channel (tilt angle is 5°). The olive oil droplet dripped at the left inlet contains Fe^{3+}, and the droplet dripped in the right inlet after 2.47 s is the KCSN solution. Above scale bars: 1 mm. (d) Schematic of HRES film attached to the inside of a silicone pipe. (e) Comparison of olive oil transportation on the original pipe, coating pipe, and HRES pipe. The pipe inclination angle is 30°. Scar bar 0.5 mm. (f) Quantitative relationship between the velocity of oil droplets and the inclined angle of the pipe. (g) Comparison of oil collection efficiency of the original pipe, coating pipe, and HRES pipe. The input mass of olive oil is 0.1 g.

To investigate the enhancement of the superamphiphobicity of the HRES compared with that of the MRES and coating (without microstructures), olive oil is employed as a representative low-surface-tension liquid for an oil repellency characterization. The contact angles of HRES and coating are 153 ± 2.1° and 154 ± 3.8°, respectively, while the contact angle of MRES is 127° (Figure 3d). According to the Cassie−Baxter equation, the apparent contact angle on the MRES can be written as[36]

$$\cos\theta_s = f_s(1 + \cos\theta_Y) - 1 \qquad (1)$$

where θ_s is the apparent contact angle, f_s is the solid fraction, and θ_Y is the intrinsic contact angle. If nanoparticles of the

liquid/solid contact fraction (f_{sn}) are introduced on the HRES, the apparent contact angle of HRES can be rewritten as[37]

$$\cos\theta_s = f_{sn}f_s(1 + \cos\theta_Y) - 1 \qquad (2)$$

Since f_{sn} is typically far less than 1, the apparent contact angle of the HRES and the coating can be largely increased compared with that of the MRES. The lower solid fraction leads to not only a higher apparent contact angle but also to less pinning of the contact line (i.e., a lower resistance to the droplet movement) and consequently to a lower droplet sliding angle (SA). Therefore, the sliding angle of the HRES (9°) is smaller than that of the coating (19°), and the oil droplet is even pinned on the MRES.

To systematically study the superamphiphobicity of the HRES, liquid droplets including hexadecane (γ = 27.5 mN/m), 35 wt % ethanol (γ = 29.8 mN/m), olive oil (32.0 mN/m), ethylene glycol (47.7 mN/m), and water (72.8 mN/m) are deposited on the HRES (Figure 3c). The apparent contact angles for all the liquids are larger than 150°, and sliding angles are lower than 10° (Figure 3e). The intrinsic contact angles are measured by depositing the same liquids on the fluorinated smooth surfaces, which are 45 ± 0.5°, 65 ± 0.5°, 77 ± 0.5°, 86 ± 0.8°, and 90 ± 1.6°, respectively (Figure S13). These large contrasts between the apparent contact angles and intrinsic contact angles demonstrate the crucial effect of the re-entrant topography in resisting the liquid invasion.

Owing to the flexibility of femtosecond laser processing, the geometry parameters such as cap diameter and pillar spacing can be well-controlled. Here, HRES with different cap diameters and pillar spacing are fabricated, and their superamphiphobicity is characterized (Figure 3f,g). For these surfaces, all the contact angles (olive oil, 4 μL) are above 150°. As the cap diameter increases from 0.05 to 0.1 mm, the sliding angle increases from 3.9 ± 0.9° to 8.7 ± 2° (pillar spacing is maintained at 0.2 mm). As the pillar spacing increases from 0.2 to 0.28 mm, the sliding angle decreases from 9.1 ± 0.9° to 4.5 ± 0.6° (the cap diameter is maintained at 0.09 mm). This is because a smaller cap diameter and a larger pillar spacing can contribute a shorter three-phase contact line, which consequently decreases the adhesion.[38−40]

Controllable Oil Manipulation on the Flexible HRES. The manipulation of low-surface-tension liquids is highly desirable for microfluidic applications ranging from microsampling detection[41,42] to microreactor engineering,[43] which has been realized on a slippery surface[44,45] but rarely reported on superamphiphobic surfaces. Here, by taking advantage of the high programmability of laser processing, the height of re-entrant micropillars can be accurately adjusted. For instance, the height of re-entrant micropillars in a designed region is lower than that of the surrounding region, and a superamphiphobic Y-type channel is obtained after a fluorination and spray coating (Figure 4a). The 4 μL 35 wt % ethanol droplet dyed with methylene blue solution rolls freely along the designed Y-path, without contamination or crossing to other areas (the surface inclination angle is 5°). Because of the difference in energy barriers of re-entrant micropillars with different heights, the droplet is blocked when it reaches the bottom of the path (Movie S2, Supporting Information). Similarly, the 4 μL olive oil droplet rolls along the designed S-path (Figure 4b, Movie S3).

Furthermore, a real-time lossless microsampling detection of oil droplets containing Fe^{3+} was realized on the HRES (Figure 4c, Movie S4). An olive oil droplet containing Fe^{3+} and a KSCN droplet are dripped at the two inlets of the Y channel, respectively. After 3.5 s, the two droplets merge at the bottom of the Y channel; a red-brown precipitate is observed, indicating the presence of Fe^{3+} in the analysis droplet.

To compare the oil manipulation performance between the HRES and slippery surface (the slippery surface is composed of MRES and silicone oil), a 4 μL 35 wt % ethanol droplet sliding test is conducted on the surfaces at the same tilt angle of 5° (Figure S14, Movie S5). As shown in Figure S14a−c, the droplet in a hemispherical shape slides downward slowly at a velocity of ~1.5 mm/s on the slippery surface; significantly different sliding behavior is observed on the HRES, where the droplet rolls down quickly in a spherical shape at a velocity of

80 mm/s. In addition, after it slides across the surface with 28 drops, the 29th droplet is pinned on the slippery surface, as the lubricant is consumed by the previous droplet sliding. Nevertheless, the velocity of the droplet rolling on the HRES remains unchanged after 50 times, demonstrating the robustness of the HRES over a slippery surface (Figure S14d).

The flexibility of superamphiphobic surfaces is of great significance in practical applications, such as wearable antifouling electronics and the textile industry. As shown in Figure S15, the HRES film has an excellent flexibility, since the HRES is fabricated on the thin bilayer of PET and PS (the total thickness is 160 μm). Moreover, with the help of a commercial adhesive, the HRES can be attached to the curved surface of a poly(tetrafluoroethylene) (PTFE) rod with a radius of 10 mm, and its superamphiphobicity remains intact (Figure S16). The olive oil can bounce off the curved surface without leaving any contaminants (Movie S6). Fifty bending-releasing tests are conducted on the HRES film, and the olive oil contact angle and sliding angle of the HRES are unchanged (Figure S17), showing a favorable robustness.

In addition, the HRES film is attached to the inside of the silicone pipe (Figure 4d). In comparison, another pipe is treated by a spray coating on the inner surface. Olive oil droplets are dripped on the 30°-tilted original pipe, coating pipe, and HRES pipe, respectively (Figure 4e, Movie S7). For the original pipe, the olive oil droplet spreads over the surface and slides down at a slow speed. For the coating pipe, although the olive oil rolls down at a faster speed, a small amount of olive oil persists during the sliding. The HRES pipe shows the best performance in oil transportation, and the olive oil rolls down quickly in a perfect spherical shape without any residue on the pipe. Under different inclination angles, the sliding velocity of the oil droplets in three pipes is further compared. As shown in Figure 4f, when the inclination angle of the pipe increases from 10° to 60°, the sliding speed of the olive oil in the original pipe increases from 0.22 to 0.9 mm/s. For the coating pipe, the driving force of the droplet (gravity along the pipe) is less than the adhesion force when the inclination angle is less than 20°, and the oil droplet is pinned because of the rose petal effect. As the angle of inclination increases, the oil droplet gradually rolls with increasing speed (the maximum speed is 72 mm/s at 60°) but still remains with a small amount of olive oil (Figure S18). For the HRES pipe, as the inclination angle increases from 10° to 60°, the rolling velocity of the oil droplet increases from 96 to 228 mm/s without any residue. The oil collection efficiency (mass of collected oil divided by input oil) of three pipes is compared in Figure 4g. Olive oil (0.1 g) is dripped on 30°-tilted three pipes, and the mass of the collected oil is weighted. Owing to the fact that the oil partially remains on the original pipe and coating pipe during the transportation, the oil transportation efficiency is only 70% and 89.5%, respectively, while the transportation efficiency of the HRES pipe reaches 100%. The experimental results indicate that the HRES pipe has an excellent performance to transport oil.

◼ CONCLUSIONS

A facile and direct approach of the laser-induced self-growing re-entrant micropillars on the PET/PS bilayer surface is proposed. A mushroom-like re-entrant micropillar can rapidly grow from the bilayer surface within 0.36 s. The cap diameter, height, and pillar spacing can be precisely and easily controlled by the femtosecond laser processing. Followed by a

fluorination and spray coating, the surface shows a super-repellency to liquids with a low surface tension liquid down to $\gamma = 27.5$ mN/m. By the construction of different HRES paths, the oil droplet manipulation is realized as well as the microsampling detection. Furthermore, by attaching the flexible HRES film to the inside of a pipe, a fast and lossless oil droplet transportation is demonstrated. This work opens a new avenue to fabricate flexible superamphiphobic surfaces, and it provides new opportunities for fields in microfabrication, microfluidics, microreactor engineering, and wearable antifouling electronics.

■ EXPERIMENTAL SECTION

Materials. The polystyrene film (150 μm thick) was purchased from Dongguan Nogard Arts & Crafts Factory. PET tape (10 μm thick and 30 μm thick) and PI tape (30 μm thick) were purchased from Kunshan kuangxun Electrical Co., Ltd. 1H,1H,2H,2H-Perfluorodecyltriethoxysilane (PFDTES), tetraethyl orthosilicate (99%), and ammonia solution (25−28% NH_3 in water) were purchased from Shanghai Aladdin Bio-Chem Technology Co., Ltd. Silicon dioxide particles (∼15 nm in diameter) were purchased from Beijing Cool Chemical Technology Co., Ltd. KCSN solution was purchased from Tianjin Yongsheng Fine Chemical Co., Ltd.

Femtosecond Laser Fabrication Method. The laser beam (104 fs, 1 kHz, 800 nm) was generated by a regenerative-amplified Ti:sapphire femtosecond laser system (Legend Elite-1K-HE, Coherent). The laser was guided onto the bilayer surface by a galvoscanner system (SCANLAB) equipped with a telecentric f-θ lens with a focal length of 63 mm. The laser spot (diameter ≈ 20 μm) is focused on the surface by adjusting the precision moving stage under the sample. The scanning path was designed by AutoCAD and then imported into the processing software Samlight.

Preparation of Fluoro-Silica Coating. The silicon dioxide particles (0.2 g) were dispersed in a solution containing ethanol (44 mL) and an aqueous ammonia solution (6 mL). The mixture was subjected to an ultrasonic treatment for 30 min. Then, the PFDTES (120 μL) and ethyl orthosilicate (30 μL) were quickly injected into the mixture under stirring at 600 rev min^{-1} at room temperature for 2 h, and a coating layer (FluoroPOS) was formed on the surface of the silicon dioxide particle.

Preparation of HRES. First, the re-entrant micropillar surface was immersed in the PFDTES solution (a mass ratio of 1:80 with ethanol) for 12 h, and then the fluoro-silica coating was uniformly sprayed on the surface by using a spray gun at a distance of 10 cm.

Characterization. The SEM images were taken by JSM-6700F, JEOL. The side-view images of the re-entrant micropillar were taken by an optical microscope (LW200-3JT). The apparent contact angle and sliding angle were measured by a contact angle system (CA100C, Innuo).

■ ASSOCIATED CONTENT

ⓈℹSupporting Information

The Supporting Information is available free of charge at https://pubs.acs.org/doi/10.1021/acs.nanolett.1c03506.

The schematic of laser-induced re-entrant micropillar array. The uniform laser-induced self-growing on bilayer surface of PET-10/PS. The random laser-induced self-growing process of PET-30. The random laser-induced

self-growing process of PI-30. Conformal ability characterization by the shrinkage of PS film on PI and PET tape. Different laser ablation effects of three tapes. The random laser-induced self-growing of re-entrant micropillar, capping layer is PI-30 and PET-30, respectively. Top view and tilted view of the SEM images show corresponding microstructures of three stages when the capping layer is PET-30. Top view and tilted view of the SEM images show corresponding microstructures of three stages when the capping layer is PI-30. Random self-grown re-entrant micropillars with increasing laser-scanning repeat circles on bilayer of PI-30/PS film. SEM images of the hierarchical re-entrant surface. The images of a water droplet on the HRES and straight pillar surface. Intrinsic contact angles of different liquids. The comparison of 35 wt % ethanol droplets sliding on the slippery surface and HRES. Optical images show the high flexibility of the HRES film. The olive oil (4 μL) drops on the curved HRES. The contact angle and sliding angle of olive oil (4 μL) as a function of the bending times. The olive oil transportation on coating pipe with inclination angle of 60° (PDF)

The laser-induced self-growing process of the re-entrant micropillars (MP4)

Droplet of 35 wt % ethanol rolls along the designed Y-type channel (MP4)

Droplet of olive oil rolls along the designed S-type channel (MP4)

Microsampling detection on the designed Y-type channel (MP4)

A comparison of 35 wt % ethanol droplets sliding on the slippery surface and HRES (MP4)

The olive oil drops on the curved HRES (MP4)

A comparison of olive oil transportation on original pipe, coating pipe, and HRES pipe (MP4)

■ AUTHOR INFORMATION

Corresponding Authors

Yanlei Hu − *Hefei National Laboratory for Physical Sciences at the Microscale, CAS Key Laboratory of Mechanical Behavior and Design of Materials, Key Laboratory of Precision Scientific Instrumentation of Anhui Higher Education Institutes, Department of Precision Machinery and Precision Instrumentation, University of Science and Technology of China, Hefei 230027, China;* ⓞ orcid.org/0000-0003-1964-0043; Email: huyl@ustc.edu.cn

Guoqiang Li − *Key Laboratory of Testing Technology for Manufacturing Process of Ministry of Education, Southwest University of Science and Technology, Mianyang 621010, China;* ⓞ orcid.org/0000-0001-8161-2065; Email: guoqli@swust.edu.cn

Dong Wu − *Hefei National Laboratory for Physical Sciences at the Microscale, CAS Key Laboratory of Mechanical Behavior and Design of Materials, Key Laboratory of Precision Scientific Instrumentation of Anhui Higher Education Institutes, Department of Precision Machinery and Precision Instrumentation, University of Science and Technology of China, Hefei 230027, China;* ⓞ orcid.org/0000-0003-0623-1515; Email: dongwu@ustc.edu.cn

Authors

Yi Yang − *Hefei National Laboratory for Physical Sciences at the Microscale, CAS Key Laboratory of Mechanical Behavior*

and Design of Materials, Key Laboratory of Precision
Scientific Instrumentation of Anhui Higher Education
Institutes, Department of Precision Machinery and Precision
Instrumentation, University of Science and Technology of
China, Hefei 230027, China; Key Laboratory of Testing
Technology for Manufacturing Process of Ministry of
Education, Southwest University of Science and Technology,
Mianyang 621010, China

Yachao Zhang − Hefei National Laboratory for Physical
Sciences at the Microscale, CAS Key Laboratory of
Mechanical Behavior and Design of Materials, Key
Laboratory of Precision Scientific Instrumentation of Anhui
Higher Education Institutes, Department of Precision
Machinery and Precision Instrumentation, University of
Science and Technology of China, Hefei 230027, China

Cong Zhang − Hefei National Laboratory for Physical
Sciences at the Microscale, CAS Key Laboratory of
Mechanical Behavior and Design of Materials, Key
Laboratory of Precision Scientific Instrumentation of Anhui
Higher Education Institutes, Department of Precision
Machinery and Precision Instrumentation, University of
Science and Technology of China, Hefei 230027, China

Yuegan Song − Key Laboratory of Testing Technology for
Manufacturing Process of Ministry of Education, Southwest
University of Science and Technology, Mianyang 621010,
China

Longfu Li − Hefei National Laboratory for Physical Sciences
at the Microscale, CAS Key Laboratory of Mechanical
Behavior and Design of Materials, Key Laboratory of
Precision Scientific Instrumentation of Anhui Higher
Education Institutes, Department of Precision Machinery and
Precision Instrumentation, University of Science and
Technology of China, Hefei 230027, China

Caiding Ni − Hefei National Laboratory for Physical Sciences
at the Microscale, CAS Key Laboratory of Mechanical
Behavior and Design of Materials, Key Laboratory of
Precision Scientific Instrumentation of Anhui Higher
Education Institutes, Department of Precision Machinery and
Precision Instrumentation, University of Science and
Technology of China, Hefei 230027, China

Nianwei Dai − Hefei National Laboratory for Physical
Sciences at the Microscale, CAS Key Laboratory of
Mechanical Behavior and Design of Materials, Key
Laboratory of Precision Scientific Instrumentation of Anhui
Higher Education Institutes, Department of Precision
Machinery and Precision Instrumentation, University of
Science and Technology of China, Hefei 230027, China

Yong Cai − Key Laboratory of Testing Technology for
Manufacturing Process of Ministry of Education, Southwest
University of Science and Technology, Mianyang 621010,
China

Jiawen Li − Hefei National Laboratory for Physical Sciences at
the Microscale, CAS Key Laboratory of Mechanical Behavior
and Design of Materials, Key Laboratory of Precision
Scientific Instrumentation of Anhui Higher Education
Institutes, Department of Precision Machinery and Precision
Instrumentation, University of Science and Technology of
China, Hefei 230027, China; orcid.org/0000-0003-
3950-6212

Jiaru Chu − Hefei National Laboratory for Physical Sciences at
the Microscale, CAS Key Laboratory of Mechanical Behavior
and Design of Materials, Key Laboratory of Precision
Scientific Instrumentation of Anhui Higher Education

Institutes, Department of Precision Machinery and Precision
Instrumentation, University of Science and Technology of
China, Hefei 230027, China; orcid.org/0000-0001-
6472-8103

Complete contact information is available at:
https://pubs.acs.org/10.1021/acs.nanolett.1c03506

Author Contributions

§These authors contributed equally to this work.

Notes

The authors declare no competing financial interest.

■ REFERENCES

(1) Karunakaran, K. P.; Suryakumar, S.; Pushpa, V.; Akula, S. Low
cost integration of additive and subtractive processes for hybrid
layered manufacturing. *Robot. Cim.-Int. Manuf.* **2010**, *26* (5), 490−
499.

(2) Kawata, S.; Sun, H.-B.; Tanaka, T.; Takada, K. Finer features for
functional microdevices. *Nature* **2001**, *412* (6848), 697−698.

(3) Bückmann, T.; Thiel, M.; Kadic, M.; Schittny, R.; Wegener, M.
An elasto-mechanical unfeelability cloak made of pentamode
metamaterials. *Nat. Commun.* **2014**, *5* (1), 1−6.

(4) Liu, X.; Gu, H.; Ding, H.; Du, X.; Wei, M.; Chen, Q.; Gu, Z. 3D
Bioinspired Microstructures for Switchable Repellency in both Air
and Liquid. *Adv. Sci.* **2020**, *7* (20), 2000878.

(5) Liu, X.; Gu, H.; Wang, M.; Du, X.; Gao, B.; Elbaz, A.; Sun, L.;
Liao, J.; Xiao, P.; Gu, Z. 3D Printing of Bioinspired Liquid
Superrepellent Structures. *Adv. Mater.* **2018**, *30* (22), e1800103.

(6) Yin, Q.; Guo, Q.; Wang, Z.; Chen, Y.; Duan, H.; Cheng, P. 3D-
Printed Bioinspired Cassie-Baxter Wettability for Controllable
Microdroplet Manipulation. *ACS Appl. Mater. Interfaces* **2021**, *13*
(1), 1979−1987.

(7) Joshi, S.; Cook, E.; Mannoor, M. S. Bacterial Nanobionics via 3D
Printing. *Nano Lett.* **2018**, *18* (12), 7448−7456.

(8) Kim, D.; Sasidharanpillai, A.; Lee, Y.; Lee, S. Self-Stratified
Versatile Coatings for Three-Dimensional Printed Underwater
Physical Sensors Applications. *Nano Lett.* **2021**, *21* (16), 6820−6827.

(9) Sánchez, C.; de Gans, B. J.; Kozodaev, D.; Alexeev, A.; Escuti, M.
J.; Van Heesch, C.; Bel, T.; Schubert, U. S.; Bastiaansen, C. W.; Broer,
D. J. Photoembossing of periodic relief structures using polymer-
ization-induced diffusion: a combinatorial study. *Adv. Mater.* **2005**, *17*
(21), 2567−2571.

(10) Stumpel, J. E.; Ziółkowski, B.; Florea, L.; Diamond, D.; Broer,
D. J.; Schenning, A. P. Photoswitchable ratchet surface topographies
based on self-protonating spiropyran−NIPAAM hydrogels. *ACS Appl.
Mater. Interfaces* **2014**, *6* (10), 7268−7274.

(11) Xue, L.; Xiong, X.; Krishnan, B. P.; Puza, F.; Wang, S.; Zheng,
Y.; Cui, J. Light-regulated growth from dynamic swollen substrates for
making rough surfaces. *Nat. Commun.* **2020**, *11* (1), 963.

(12) Li, T.; Ma, T.; Li, J.; Chen, S.; Ma, X.; Yin, J.; Jiang, X.
Micropatterns Fabricated by Photodimerization-Induced Diffusion.
Adv. Mater. **2021**, *33*, e2007699.

(13) Zhang, Y.; Li, Y.; Hu, Y.; Zhu, X.; Huang, Y.; Zhang, Z.; Rao,
S.; Hu, Z.; Qiu, W.; Wang, Y.; Li, G.; Yang, L.; Li, J.; Wu, D.; Huang,

W.; Qiu, C.; Chu, J. Localized Self-Growth of Reconfigurable Architectures Induced by a Femtosecond Laser on a Shape-Memory Polymer. *Adv. Mater.* **2018**, *30* (49), e1803072.

(14) Tuteja, A.; Choi, W.; Ma, M.; Mabry, J. M.; Mazzella, S. A.; Rutledge, G. C.; McKinley, G. H.; Cohen, R. E. Designing superoleophobic surfaces. *Science* **2007**, *318* (5856), 1618−1622.

(15) Choi, J.; Jo, W.; Lee, S. Y.; Jung, Y. S.; Kim, S. H.; Kim, H. T. Flexible and Robust Superomniphobic Surfaces Created by Localized Photofluidization of Azopolymer Pillars. *ACS Nano* **2017**, *11* (8), 7821−7828.

(16) Liu, T. L.; Kim, C.-J. C. Turning a surface superrepellent even to completely wetting liquids. *Science* **2014**, *346* (6213), 1096−1100.

(17) Tuteja, A.; Choi, W.; Mabry, J. M.; McKinley, G. H.; Cohen, R. E. Robust omniphobic surfaces. *Proc. Natl. Acad. Sci. U. S. A.* **2008**, *105* (47), 18200−18205.

(18) Yun, G.-T.; Jung, W.-B.; Oh, M. S.; Jang, G. M.; Baek, J.; Kim, N. I.; Im, S. G.; Jung, H.-T. Springtail-inspired superomniphobic surface with extreme pressure resistance. *Sci. Adv.* **2018**, *4* (8), eaat4978.

(19) Mazumder, P.; Jiang, Y.; Baker, D.; Carrilero, A.; Tulli, D.; Infante, D.; Hunt, A. T.; Pruneri, V. Superomniphobic, transparent, and antireflection surfaces based on hierarchical nanostructures. *Nano Lett.* **2014**, *14* (8), 4677−4681.

(20) Yao, X.; Gao, J.; Song, Y.; Jiang, L. Superoleophobic Surfaces with Controllable Oil Adhesion and Their Application in Oil Transportation. *Adv. Funct. Mater.* **2011**, *21* (22), 4270−4276.

(21) Wang, W.; Du, X.; Vahabi, H.; Zhao, S.; Yin, Y.; Kota, A. K.; Tong, T. Trade-off in membrane distillation with monolithic omniphobic membranes. *Nat. Commun.* **2019**, *10* (1), 3220.

(22) Huang, J. Y.; Lai, Y. K.; Pan, F.; Yang, L.; Wang, H.; Zhang, K. Q.; Fuchs, H.; Chi, L. F. Multifunctional superamphiphobic TiO2 nanostructure surfaces with facile wettability and adhesion engineering. *Small* **2014**, *10* (23), 4865−4873.

(23) Yan, H.; Abdul Rashid, M. R. B.; Khew, S. Y.; Li, F.; Hong, M. Wettability transition of laser textured brass surfaces inside different mediums. *Appl. Surf. Sci.* **2018**, *427*, 369−375.

(24) Shabanian, S.; Khatir, B.; Nisar, A.; Golovin, K. Rational design of perfluorocarbon-free oleophobic textiles. *Nat. Sustain.* **2020**, *3* (12), 1059−1066.

(25) Li, F.; Wang, Z.; Huang, S.; Pan, Y.; Zhao, X. Flexible, Durable, and Unconditioned Superoleophobic/Superhydrophilic Surfaces for Controllable Transport and Oil-Water Separation. *Adv. Funct. Mater.* **2018**, *28* (20), 1706867.

(26) Xu, Z.; Zhao, Y.; Wang, H.; Wang, X.; Lin, T. A superamphiphobic coating with an ammonia-triggered transition to superhydrophilic and superoleophobic for oil-water separation. *Angew. Chem., Int. Ed.* **2015**, *54* (15), 4527−4530.

(27) Chen, L.; Guo, Z.; Liu, W. Biomimetic Multi-Functional Superamphiphobic FOTS-TiO2 Particles beyond Lotus Leaf. *ACS Appl. Mater. Interfaces* **2016**, *8* (40), 27188−27198.

(28) Jiang, S.; Hu, Y.; Wu, H.; Zhang, Y.; Zhang, Y.; Wang, Y.; Zhang, Y.; Zhu, W.; Li, J.; Wu, D.; Chu, J. Multifunctional Janus Microplates Arrays Actuated by Magnetic Fields for Water/Light Switches and Bio-Inspired Assimilatory Coloration. *Adv. Mater.* **2019**, *31* (15), 1807507.

(29) Jiang, S.; Hu, Y.; Wu, H.; Li, R.; Zhang, Y.; Chen, C.; Xue, C.; Xu, B.; Zhu, W.; Li, J.; Wu, D.; Chu, J. Three-Dimensional Multifunctional Magnetically Responsive Liquid Manipulator Fabricated by Femtosecond Laser Writing and Soft Transfer. *Nano Lett.* **2020**, *20* (10), 7519−7529.

(30) Yang, J.; Luo, F.; Kao, T. S.; Li, X.; Ho, G. W.; Teng, J.; Luo, X.; Hong, M. Design and fabrication of broadband ultralow reflectivity black Si surfaces by laser micro/nanoprocessing. *Light: Sci. Appl.* **2014**, *3* (7), e185−e185.

(31) Liu, X.-Q.; Bai, B.-F.; Chen, Q.-D.; Sun, H.-B. Etching-assisted femtosecond laser modification of hard materials. *Opto-Electron. Adv.* **2019**, *2* (9), 19002101−19002114.

(32) Song, Y.; Jiang, S.; Li, G.; Zhang, Y.; Wu, H.; Xue, C.; You, H.; Zhang, D.; Cai, Y.; Zhu, J.; Zhu, W.; Li, J.; Hu, Y.; Wu, D.; Chu, J. Cross-Species Bioinspired Anisotropic Surfaces for Active Droplet Transportation Driven by Unidirectional Microcolumn Waves. *ACS Appl. Mater. Interfaces* **2020**, *12* (37), 42264−42273.

(33) Tiaw, K. S.; Goh, S. W.; Hong, M.; Wang, Z.; Lan, B.; Teoh, S. H. Laser surface modification of poly(epsilon-caprolactone) (PCL) membrane for tissue engineering applications. *Biomaterials* **2005**, *26* (7), 763−769.

(34) Liu, H.; Wang, Y.; Huang, J.; Chen, Z.; Chen, G.; Lai, Y. Bioinspired Surfaces with Superamphiphobic Properties: Concepts, Synthesis, and Applications. *Adv. Funct. Mater.* **2018**, *28* (19), 1707415.

(35) Zhao, Y.; Su, Y.; Hou, X.; Hong, M. Directional sliding of water: biomimetic snake scale surfaces. *Opto-Electron. Adv.* **2021**, *4* (4), 210008−210008.

(36) Cassie, A.; Baxter, S. Wettability of porous surfaces. *Trans. Faraday Soc.* **1944**, *40*, 546−551.

(37) Li, X.; Wang, D.; Tan, Y.; Yang, J.; Deng, X. Designing Transparent Micro/Nano Re-Entrant-Coordinated Superamphiphobic Surfaces with Ultralow Solid/Liquid Adhesion. *ACS Appl. Mater. Interfaces* **2019**, *11* (32), 29458−29465.

(38) Pan, S.; Guo, R.; Bjornmalm, M.; Richardson, J. J.; Li, L.; Peng, C.; Bertleff-Zieschang, N.; Xu, W.; Jiang, J.; Caruso, F. Coatings super-repellent to ultralow surface tension liquids. *Nat. Mater.* **2018**, *17* (11), 1040−1047.

(39) Deng, X.; Mammen, L.; Butt, H.-J.; Vollmer, D. Candle soot as a template for a transparent robust superamphiphobic coating. *Science* **2012**, *335* (6064), 67−70.

(40) Panter, J.; Gizaw, Y.; Kusumaatmaja, H. Multifaceted design optimization for superomniphobic surfaces. *Sci. Adv.* **2019**, *5* (6), eaav7328.

(41) Cui, Z.; Xiao, L.; Li, Y.; Zhang, Y.; Li, G.; Bai, H.; Tang, X.; Zhou, M.; Fang, J.; Guo, L.; Liu, S.; Xiao, C.; Cao, M. A fishbone-inspired liquid splitter enables directional droplet transportation and spontaneous separation. *J. Mater. Chem. A* **2021**, *9* (15), 9719−9728.

(42) Fang, J.; Zhang, Y.; Xiao, L.; Jiao, Y.; Tang, X.; Cheng, H.; Cui, Z.; Li, X.; Li, G.; Cao, M.; Zhong, L. Self-Propelled and Electrobraking Synergetic Liquid Manipulator toward Microsampling and Bioanalysis. *ACS Appl. Mater. Interfaces* **2021**, *13* (12), 14741−14751.

(43) Wong, W. S.; Liu, G.; Tricoli, A. Superamphiphobic Bionic Proboscis for Contamination-Free Manipulation of Nano and Core-Shell Droplets. *Small* **2017**, *13* (14), 1603688.

(44) Luo, X.; Lai, H.; Cheng, Z.; Liu, P.; Li, Y.; Yu, X.; Liu, Y. Slippery shape memory polymer arrays with switchable isotropy/anisotropy and its application as a reprogrammable platform for controllable droplet motion. *Chem. Eng. J.* **2021**, *403*, 126356.

(45) Wang, J.; Gao, W.; Zhang, H.; Zou, M.; Chen, Y.; Zhao, Y. Programmable wettability on photocontrolled graphene film. *Sci. Adv.* **2018**, *4* (9), eaat7392.